

Chapter 2

Dynamical Systems

2.1 Introduction

Anything that is changing with time is called dynamic. A system whose states are changing with respect to time is called a dynamic system. In general, a dynamic system is described by differential equations. The precise control of high speed motion demands a realistic dynamic model of the robot arm. The dynamic equations of motion of a general robotic arm is rather complex. There are different approaches used by researchers to derive the equations of motion for robotic systems. The first is the Lagrange-Euler formulation (Schilling 1990) based on the concept of generalised coordinates, energy, and generalised force. An alternative approach is the recursive Newton-Euler formulation, which is computationally more efficient (Asada and Stoline 1986; Fu et al. 1987).

Using the D' Alembert's principle of the fundamental classical laws of motion, dynamics of arms can be derived by summing all of the forces acting on the coupled rigid bodies that form the robot arm. But the Lagrangian derivation of the dynamics has the advantage of requiring only the kinetic and potential energies of the system. Therefore, Lagrangian analysis is employed to compute the equations of motion.

The Lagrangian, L , is defined based on the notion of generalised coordinates, energy and generalised forces, as the difference between the kinetic energy and potential energy of the system:

$$L(q, \dot{q}) = K(q, \dot{q}) - V(q) \quad (2.1)$$

where K is the kinetic energy and V is the potential energy of the system, q represents the joint variables, $\dot{q} = dq/dt$ represents the joint velocities. The general equations of motion of a robotic arm can be defined in terms of Lagrangian function as follows:

$$\frac{d}{dt} \frac{\partial}{\partial \dot{q}_i} L(q, \dot{q}) - \frac{\partial}{\partial q_i} L(q, \dot{q}) = F_i \quad (2.2)$$

where F_i , $i = 1, 2, \dots, n$, is the generalized forces acting on the i th joint. The Lagrangian equation of robot dynamics consists of n -second order nonlinear differential equations in the vector of joint-space of q . To derive any dynamic equation for any robotic system, we need to formulate expressions for kinetic energy K , potential energy V , and generalised forces F . The computation of the total kinetic energy of a robotic arm $K(q, \dot{q})$ in Lagrangian function is the most complicated term. The potential energy $V(q)$ is the gravitational forces. The generalized forces are the residual forces acting on the robot arm.

2.2 Dynamics of Robot Manipulator

The dynamic equation of an n -axis robot arm can be derived from Lagrangian function in (2.2) when the detailed expressions for the kinetic energy, potential energy and generalised forces are available. The general dynamic model of the robot arm can be described by the following equation with the joint variables q and actuator torques τ :

$$\sum_{j=1}^n D_{ij}(q)\ddot{q}_j + \sum_{k=1}^n \sum_{j=1}^n C_{kj}^i(q)\dot{q}_k\dot{q}_j + h_i(q) + b_i(\dot{q}) = \tau_i, \quad i = 1, \dots, n \quad (2.3)$$

The first term $D_{ij}(q)\ddot{q}_j$ is an acceleration term that represents the inertial forces and torques generated by the motion of the links of the arm. The second term $C_{kj}^i(q)\dot{q}_k\dot{q}_j$ is a product velocity term associated with Coriolis and centrifugal forces. The third term $h_i(q)$ is the position term representing loading due to gravity. The fourth term $b_i(\dot{q})$ is a velocity term representing the friction acting opposite to the motion of the arm. The n separate scalar equations in (2.3) can be written as a single vector equation as follows:

$$D(q)\ddot{q} + c(q, \dot{q}) + h(q) + b(\dot{q}) = \tau; \quad (2.4)$$

The term $c(q, \dot{q})$ is called the velocity coupling vector. There are two distinct types of inter-axis velocity coupling arising from here, which can be expanded into two terms as follows:

$$c(q, \dot{q}) = \sum_{k=1}^n C_{kk}^i(q)\dot{q}_k^2 + \sum_{k=1}^n \sum_{j \neq k}^n C_{kj}^i(q)\dot{q}_k\dot{q}_j \quad (2.5)$$

The first summation corresponds to squared velocity terms associated with centrifugal forces acting on joint i due to motion of joint k . The second summation corresponds to product velocity terms associated with Coriolis forces acting on joint i due to the combined motions of joints k and j such that $j \neq k$.

2.3 Dynamics of Flexible-Arm

To design a flexible arm efficiently, whether intended for a specific application or for a range of applications, several factors need to be considered. These include the strength and flexibility of the arm, fast speed and acceleration capability, good payload requirements, choice of suitable actuator and sensing equipment for the control mechanisms intended to be employed. The problem of oscillatory behaviour due to arm flexibility has traditionally been solved by mechanically stiffening the arm. However, this leads to an increase in the weight of the arm. Thus, a conventional industrial robot arm does not achieve the objective of the lighter weight requirement of the flexible arm.

The issue of flexible arm design and control thus primarily caters for the design of controllers to either compensate for the structural flexibility or to be robust in the presence of structural flexibility. It has been shown that using joint position and velocity sensors in a feedback control scheme for a rigid robot is adequate to ensure satisfactory performance (Khosla and Kanade 1988; Seraji and Moya 1987). However, these sensors may not be sufficient to provide the necessary information for the control of the elastic behaviour of a flexible arm. In addition to measuring joint position and velocity, it is desirable to obtain the state of the end-point as well. Although the deflection information of the arm can be theoretically determined if the dynamic model of the system is available, this will require high computing power and speed for on-line computation in addition to the uncertainties usually associated with formulating the dynamic model of the flexible arm. This argument for control purposes leads to the requirement of a suitable measuring system for the flexible arm's end-point.

A description and dynamic characterisation of the flexible arm utilised to verify different intelligent control strategies is presented in this chapter. Similar experimental arms have been constructed in the past (Cannon and Schmitz 1984; Hastings and Ravishankar 1988). The principal originality of the arrangement presented here is that the deflection of the flexible arm is measured and controlled using an accelerometer at the end-point. The following sections are intended to recall, in an abbreviated form, the design procedures of a laboratory facility for experimental study of a single-link flexible arm using end-point acceleration feedback (Azad 1994; Tokhi and Azad 1997). The main purpose of the design procedure is to relate a set of criteria which are useful in the design procedure, such as accuracy of end-point, allowable payload mass, maximum joint velocity, maximum joint acceleration and operating bandwidth of the arm. This will lead to preliminary results of the arm parameters. The actuating system is also studied and incorporated into the design procedure. Moreover, the design procedure will also indicate the significance of flexibility for a range of specifications.

2.3.1 Strength and Stiffness

Arm strength is the ability to withstand loads, which create stress in the system. These loadings arise from attempts to move and stop the arm and to maintain a position in gravity or other force fields. These loadings limit the capability of the arm to perform its specified functions by limiting the speed with which it can move. This speed limitation can yield a basis for comparison against stiffness limitations. The stiffness itself is the tendency of the arm to resist deflections, which may take the form of vibrations. For a distributed system such as a flexible arm, these may take place at an infinite number of frequencies. Strength is seemingly a more compelling requirement since inadequate provisions for strength can result in catastrophic failures if a component fractures.

Arm strength and stiffness are qualitatively affected in the same way by a number of parameters including payload mass, arm's material density and length and dimensions of the cross section. Varying one of these parameters to make the arm stronger will result in a stiffer arm. Other parameters directly affecting only strength include the maximum allowable stress for the arm material, inertial loading from accelerating the arm and its payload, and the gravity or other constant body forces present in the environment. Stiffness is characterised by the natural frequencies, and its magnitude is additionally affected by the value of the Young's modulus for the material used.

Two other factors influencing characterisation of an arm are rigidity and flexibility. The rigidity of the system can be checked by using a rule of thumb (Book 1984) which can be summarized as: if the servo frequency ω_s of a controller is less than a third of the first resonance frequency of the arm $[\omega_1]$, then the arm can be considered as rigid. If the servo frequency is between $\omega_1/3$ and $\omega_1/2$ then vibration will occur but will be well damped. If the servo frequency is greater than $\omega_1/2$, oscillations with insufficient damping will result. This will help to indicate the significance of flexibility and rigidity for a range of specifications.

For the single-link arm considered, there are only two parameters, namely thickness and width that can be altered to increase the strength of the arm. The minimum thickness, as discussed later, will limit the stability of the arm. The arm can be considered as a pinned-free flexible beam, with a lumped inertia at the hub, which can bend freely in the horizontal plane but is stiff in vertical bending and torsion. To avoid the difficulties arising in the case of a beam with time-varying length, the length l of the arm is assumed to be fixed. Moreover, shear deformation, rotary inertia and effect of axial force are also neglected. A schematic representation of the single-link flexible arm system under consideration is shown in Fig. 2.1, where E, I, ρ, M_p and I_h are the Young's modulus, the area moment of inertia, the mass density per-unit length, payload mass and hub inertia respectively.

For a given value of payload mass at the end point of the arm and a desired linear acceleration at the centre of gravity of the payload mass, the desired moment at the joint (hub) can be calculated as (Book 1984)

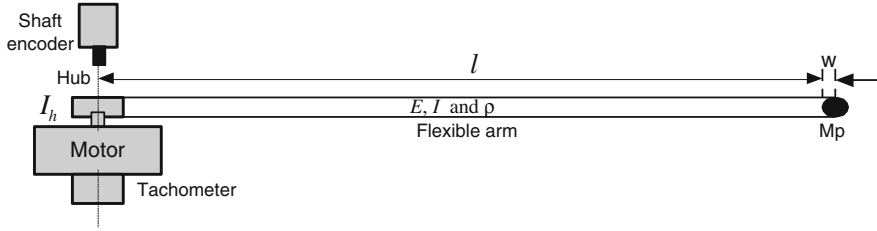


Fig. 2.1 Outline of the flexible arm system

$$\sigma = \alpha M_p w + \alpha M_p l + \frac{\rho}{2} \left[\frac{\alpha - g}{l + w} + g \right] l^2 - \frac{\rho(\alpha - g)}{6(l + w)} l^3 + \frac{I_h \alpha}{l + w} \quad (2.6)$$

where,

σ = required moment at the hub of the flexible arm,

α = linear acceleration at the centre of gravity of the payload mass,

w = offset between the centre of gravity of the payload mass and the end-point of the arm,

g = acceleration due to gravity.

For a given flexible arm, the maximum torque, which can be applied to the joint is given by

$$\tau_{\max} = \frac{\sigma_{\max} I}{C} \quad (2.7)$$

where,

τ_{\max} = maximum applied torque,

σ_{\max} = maximum tensile stress (without changing the shape). This depends upon the material used for the flexible arm construction;

I = second moment of inertia of the arm,

C = half of the thickness of the arm (thickness/2).

For the arm to be strong enough to handle the desired torque, the following criterion must be satisfied

$$\sigma_{\max} \geq \sigma \quad (2.8)$$

where equality applies to the optimum structure of the arm. It follows from Eq. (2.7) that the minimum thickness of the flexible arm depends upon the amount of torque required to be applied at the joint, i.e. upon the linear acceleration at the centre of gravity of the payload mass.

2.3.2 Safety Factor

The safety factor for the arm design can be defined as

$$SF = \frac{\sigma_{\max}}{\sigma} \quad (2.9)$$

For optimum design, the safety factor is to be unity. Figure 2.2 shows the relation between end-point acceleration α and thickness T of the arm with various values of safety factor for a given material (e.g. Aluminium alloy) with a payload mass of 10 g, length of 0.96 m, and hub inertia of $5.86 \times 10^{-4} \text{ kgm}^2$. For a given end-point acceleration and safety factor, the thickness of the flexible arm can be found from this diagram for a specific configuration.

The design and development of a flexible arm includes three areas (Tokhi and Azad 1997): (a) design and construction of the mechanical structure; (b) choice of suitable transducers for the specific application; (c) development of required amplifiers and processing circuits and their calibration.

For the flexible arm utilized in this research as an experimental rig, a printed circuit armature type motor is used as the drive actuator due to its low inertia, low inductance and physical structure, which allows to be connected to the flexible arm. The system incorporates an LA5600 amplifier/controller for controlling the required dc-current driving the motor. This is due to its several features such as motor clamping, directional clamping and output current monitoring provision. The details of LA5600 are presented in Sect. 2.3.5.

For measurement of angular movement, the developed processing circuit is able to produce both digital and analogue outputs at the same time. This enables the use of analogue output from a 16-bit D/A as a feedback signal to the amplifier/controller and digital output to the computer. This circuit can be modified to control a microprocessor where the 8-bit output of the THCT2000 could be directly connected with the computer's data bus. The system uses a new type of velocity measurement transducer instead of the conventional tachometer. A special

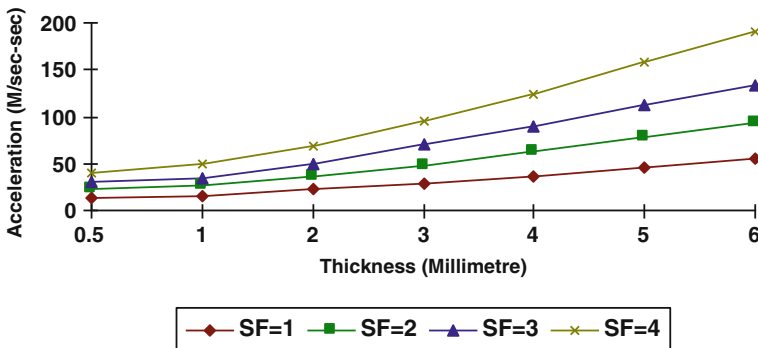


Fig. 2.2 Relation between end-point acceleration and required thickness of the flexible arm

feature of this transducer is that the output is totally free from any noise induced from commutator friction, which is very important for low-level feedback signals. Moreover, the inertia for this system is very small. In selecting the type of accelerometer and strain gauge, size, weight and frequency range constraints are considered strictly. The accelerometer utilised includes a built-in FET source follower, which allows for a lower output impedance level.

Due to the irregular shape of the flexible arm hub, the hub inertia is measured experimentally. This is important for modelling and simulation of the system. Motor friction is also measured experimentally to verify the supplier's data-sheet, which has been found to be 0.011 Nm. However, this parameter is not considered in the model because the effect of friction is not significant as compared to the applied torque.

Noise and interference have been a serious problem than others during testing and experiments. To overcome this, a linear amplifier is used and all the signal amplifiers are powered from a battery instead of from the mains power supply.

Pentium I microcomputer in conjunction with an ADC-44d I/O board is used with the flexible arm system. The experimental setup requires one analogue output to the motor drive amplifier, four analogue inputs from the hub-angle and velocity transducer, accelerometer and motor current sensor. The interface board is used with a conversion time of 3 μ s for A/D conversion and settling time of 20 μ s for D/A conversion, which are satisfactory for the system under consideration. The details of the ADC-44d I/O board are presented in [Sect. 2.3.7](#).

A more detailed description of the flexible arm system is given in the next section.

2.3.3 Experimental Flexible Arm

The experimental rig constituting the flexible arm system consists of two main parts: a flexible arm and measuring devices. The flexible arm contains a flexible link driven by a printed armature motor at the hub. The measuring devices are shaft encoder, tachometer, accelerometer and strain gauges along the length of the arm. The shaft encoder, tachometer and accelerometer are utilised in this work. The experimental rig is shown in [Fig. 2.3a](#) and the schematic diagram of the rig is shown in [Fig. 2.3b](#).

The shaft encoder is used for measuring the hub angle of the arm. A tachometer is used for measurement of the hub velocity. An accelerometer is located at the end-point of the flexible arm measuring the end-point acceleration. The flexible arm is constructed using a piece of thin aluminium alloy. The parameters of the flexible arm are given in [Table 2.1](#).

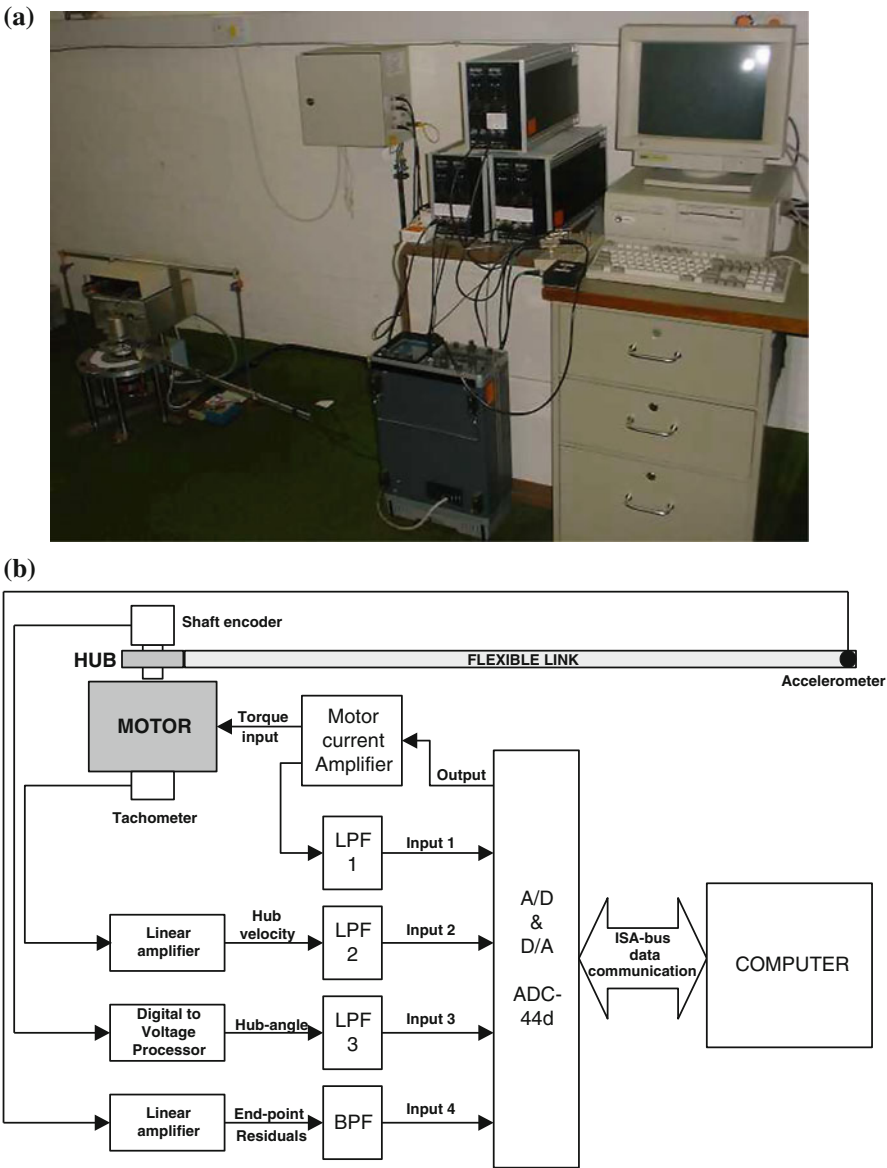


Fig. 2.3 Experimental rig Flexible arm (a); Schematic diagram of the experimental rig (b)

2.3.4 Printed Armature Motor

The experimental rig is equipped with a U9M4AT type printed circuit motor driving the flexible arm. The specifications of the motor are given in Table 2.2.

Table 2.1 Parameters and characteristics of the flexible arm system

Parameter	Value
Length	960.0 mm
Width	19.008 mm
Thickness	3.2004 mm
Mass density per unit volume	2,710 kgm ⁻³
Second moment of inertia, I	5.1924×10^{-11} m ⁴
Young modulus, E	71×10^9 Nm ⁻²
Moment of inertia, I_b	0.04862 kgm ²
Hub inertia, I_h	5.86×10^{-4} kgm ²

Table 2.2 Specifications of the U9M4AT motor

Parameters	Unit	Value
Peak torque	Nm	3.075
Peak current	A	72.0
Peak acceleration	Krad.s ⁻²	52.3
Continuous torque	Nm	0.325
Continuous current	A	8.68
Maximum terminal voltage	V	22.9
No load speed	RPM	4593
Power output	W	101.7
Torque constant	Nm/A	0.043
Back e.m.f. constant	V/Krpm	4.5
Armature resistance	Ω	0.66
Moments of inertia	Nm.s ²	5.88×10^{-5}
Armature inductance	μ H	<100
Mechanical time constant	μ s	20.52
Electrical time constant	μ s	<0.15
Voltage constant	V/Krpm	2.25

This type of motor gives significant performance advantages for motion control applications, which can be listed as follows (Azad 1994):

- It gives high acceleration since it is able to produce high torque combined with low armature inertia. This means shorter cycle times, more displacement per second and higher throughput.
- It has a very low inductance, which leads to a negligible electrical time constant and a short mechanical time constant (less than one millisecond). This implies almost instantaneous application of full torque. This is a key to fast motion and accurate tracking.
- It does not have armature associated torque loss due to its construction and as a result delivers more torque over its entire speed range. Moreover, the torque is almost constant throughout its speed range. These properties provide a non-varying transfer function over the entire operating range of the motor.
- Due to the absence of any iron in the rotor and a large number of commutator bars and slots, extremely smooth torque with no “cogging” is achieved.

- With the non-magnetic printed circuit armature and axial magnetic field, the problem of demagnetisation of the permanent magnet is virtually eliminated. Most printed armature motors are rated for a peak current of 10 times the continuous rating. This property enables them to produce rapid acceleration and deceleration when higher than the rated torque is usually required.
- As the inductance is nearly zero, there is no stored energy in the armature to be dissipated during commutation. This eliminates arcing, which is the major cause of brush wear. This increases the reliability in operation and life expectancy.

2.3.5 Motor Drive Amplifier

Linear amplifiers may be classified as either unidirectional with dynamic breaking capability or bi-directional. For a unidirectional motor, deceleration is only dependent on system friction and viscous damping, which takes a longer time to stop the motor. This can be modified by introducing a circuit which shorts the motor terminals when the motor current becomes zero, allowing a negative current to circulate in the armature, thus stopping the motor. However, the drive amplifier used is a bi-directional one because the motor needs to be driven in both directions to control the arm vibration. The motor driver used is the LA5600 manufactured by Electro-Craft Corporation. This motor drive amplifier (current amplifier) delivers a current proportional to the input voltage. It serves as a velocity/position controller as well as a motor driver. The reasons for using this amplifier/controller can be listed as follows:

1. The main objective is to control the flexible arm by applying a controlled amount of torque at the arm hub. This amplifier/controller can be used in torque-controlled mode. That is, for a given amount of input voltage it can produce a proportional current output to the motor.
2. For off-line identification of the system, it is needed to operate the system in a joint based position and velocity feedback system. With this amplifier/controller, such a system can be implemented by feeding back the tachometer and shaft encoder output to the amplifier.
3. This amplifier has a four clamp facility, which can be used to limit or restrict the function of the amplifier and consequently of the entire system to accommodate various application requirements. The inhibit (INH) clamp is used to disable the amplifier by turning all transistors in the output stage OFF when the clamp is activated. The motor hold (MHO) clamp is used to stop the motor by effectively driving the amplifier input signal to zero. It decelerates the motor and load to zero speed as fast as possible and then holds the motor when stopped. The system resists external torque applied to the motor shaft. These two clamps could be used to stop the motor at any extreme operational situation by disconnecting them from the ground (COM). The forward direction (FAC) clamp and reverse direction (RAC) clamp affect the specific direction of motor movement. When one of these clamps modes is activated, it prevents movements of the motor in

that direction. These forward and reverse direction clamps can be used by wiring through normally closed travel limit micro switches. This will stop the flexible arm when moved beyond its range of movement.

4. There are three other output signals from this amplifier/controller, which could be used as input to the controller or for monitoring purposes. The first one is the motor velocity output (MVO) signal, which is an analogue voltage signal and is proportional to the actual instantaneous motor speed. The second one is the motor current output (MCO), which is a voltage proportional to the actual motor current. Knowing the amount of current output from the amplifier, the applied torque can be calculated by multiplying the current (I_a) with motor torque constant (K_t). The third output is the system status output (SSO), which is a logic level signal.

2.3.6 Accelerometer

There are two types of accelerometer commonly in use: (a) strain gauge type accelerometers; and (b) piezoelectric accelerometers. Due to weight and size constraints, the flexible arm system used in this work incorporates a piezoelectric type transducer. Table 2.3 shows the specifications of the accelerometer used.

In this type of accelerometer, the crystal-sensing element is isolated from the case and compressed or sheared between the accelerometer base and a seismic mass. A dynamic force applied to the accelerometer in either direction along its sensitive axis causes the crystal to generate a charge proportional to the acceleration. The generated voltage can be represented as

$$v = \frac{DM}{C}A \quad (2.10)$$

where D , M , C , A are the piezoelectric constants of the material, the mass of the seismic mass, the capacitance and the acceleration respectively.

Table 2.3 Specifications of the 303A03 accelerometer

Parameters	Unit	Value
Range	g	±500
Resolution	g	0.01
Sensitivity	mV/g	10
Frequency range	Hz	1–10,000
Output impedance	Ω	100
Linearity	%	1
Transverse sensitivity (max)	%	5
Excitation voltage	V	18–24
Excitation current	mA	2–20
Weight	g	2

2.3.7 Computer Interfacing

The computer used for this experimental rig was an IBM-PC compatible Pentium I 100 MHz CPU. Data acquisition and control was accomplished through the utilization of an ADC-44d I/O board. This board provides a direct interface between the microcomputer and the actuators and transducers..

The ADC-44d board contains an NEC μ PD71055 device, which is equivalent to an Intel i8255 PIO. This device produces 24 programmable digital I/O channels. It is suitable for sensing the presence of TTL driving connections. It contains a 12-bit A/D converter with a conversion time of $3\mu\text{s}$. Various configurations of its CMOS multiplexer enable it to receive different numbers of input channels with different voltage ranges. A/D conversion can be initiated by one of three possible means: using a software convert command, applying an external TTL logic level signal or by programming the NEC μ PD71055 chip. The ADC44d is able to generate an interrupt when one of three independent conditions has occurred: when an A/D conversion is completed, when an overrun condition has occurred or when a given number of counts have finished. The board contains two independent voltage output channels, each with its own 12-bit D/A converter, which can produce an output from $\pm 10\text{ V}$ to $\pm 50\text{ mV}$. For time related digital I/O applications, the NEC μ PD71055/NEC μ PD71054 counter/timer chip provides the ADC-44d with three independent 16-bit channels that can be used for such counter/timer functions as event counting, frequency measurement, single pulse output and time proportional output. The board is mapped into the microcomputer's I/O channel structure as a block of 16 consecutive bytes, addressable on any unoccupied 16-byte boundary from address 200H to 3FFH.

2.3.8 Operating Characteristics

Many systems and signal sources have non-linear characteristics associated with actuation and sensing. Possible sources and types of input (actuation) non-linearity and output (sensor) non-linearity are illustrated in Fig. 2.4.

A typical input non-linearity is the dead-zone $\pm U_d$. This represents a signal level below which no actuation signal $u_{\text{act}}(t)$ is sent to the system. The signal $u(t)$ must be designed to ensure that it has a minimum amplitude in this region.

The characteristics of frictional forces between two contacting surfaces often depend on several factors including the composition of the surfaces, the pressure between two surfaces and their relative velocity. An exact mathematical description of the frictional forces is thus difficult to obtain (Kuo and Tal 1978). The amount of friction associated with the motor has previously been determined experimentally (Azad 1994). The measured friction (viscous coefficient B) was found to be $0.029\text{ mNm/rad/second}$.

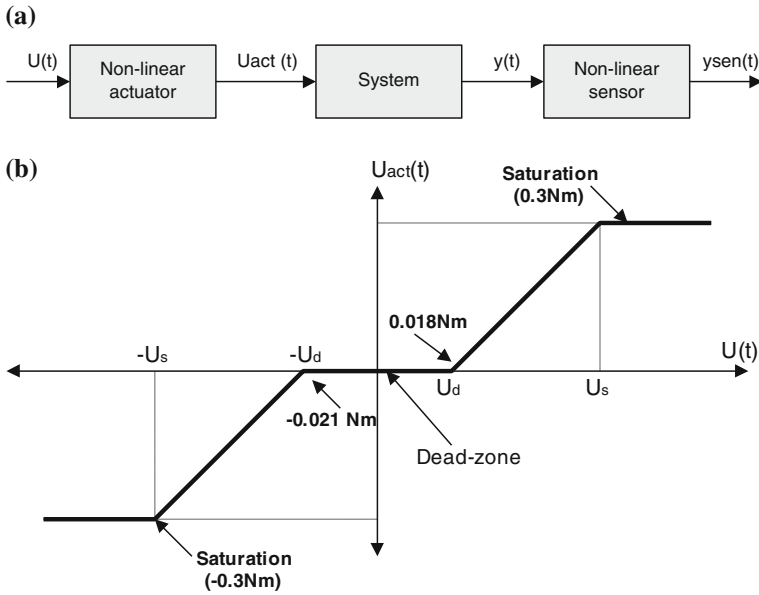


Fig. 2.4 Non-linear characteristics associated with actuation and sensing. Actuation and sensing (a); Input non-linearity with saturation limits (b)

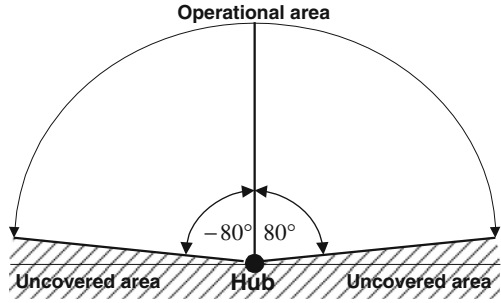
The torque required to eliminate the *dead-zone* has been found to be at least ± 10.0 mNm. The presence of the flexible beam, including the clamp, would obviously affect the *dead-zone*. This implies that a *dead-zone* compensator would be required. Thus, if the torque has low amplitude components, which are within the *dead-zone*, a minimum amount of torque should be maintained outside the *dead-zone*. It is noted in Fig. 2.4b that the characteristic of the *dead-zone* of the flexible arm lies between $+18$ and -21 mNm. By considering the error between both, the angle of demand and position and the hub-velocity, the compensation torque could be started.

The flexible arm hub-movements is defined to be in the range of $\pm 80^\circ$ of angle only, as illustrated in Fig. 2.5. The uncovered angle here is the undesired angles, which are beyond the defined range.

2.4 Previous Research and Developments

Research in the area of flexible arm systems has been carried out for over 20 years. These range from a single-link arm rotating about a fixed axis to three-dimensional multi-link arms. However, most of the experimental work is limited to single-link arm systems. This is due to the complexity of multi-link arm systems.

Fig. 2.5 Operational range of the flexible arm



Tokhi and Azad (1996a) have given a brief description of previously developed methods of modelling of flexible arms. These can be classified as

- Lagrange's equation and modal expansion (Ritz-Kantrovitch),
- Lagrange's equation and finite element method,
- Euler-Newton's equation and modal expansion method,
- Euler-Newton's equation and finite element method,
- Singular perturbation and frequency domain techniques.

In Lagrange's equation and modal expansion method, the model is in the form of a summation of modes. Each mode is a product of two functions: one is a function of distance along the length of the arm, the other is a function of generalised co-ordinates dependent upon time. The model contains an infinite number of modes. In practice, a finite number of modes is used. The Lagrange's equation and finite element method is similar to the Lagrange's equation and modal expansion method. In Lagrange's equation and finite element method, the generalised co-ordinates are the displacement and/or slope at specific points along the arm.

The Euler-Newton's method is a more direct method of calculating system dynamics. The derivatives of linear and angular momentum are derived explicitly. Newton's second law is applied to equate these terms to the applied forces and torques. The linear and angular momentum of arm is the unknown. These are expressed in terms of assumed modes of finite elements. This leads to a dynamic model containing time dependent elements, which relate to the applied forces and torques. The basic approach in the Euler-Newton's equation and assumed mode method is to divide the system into a number of finite elements and balance each element dynamically. This method can be tedious if the total number of elements is large. The advantage of this method is that it is easier to include non-linear effects without complicating the basic linear model.

In the singular perturbation technique, the characteristic modes of the system are separated into two groups. These include a set of low-frequency, or slow modes, and a set of high frequency, or fast modes. In a flexible arm system, the rigid body modes are the low frequency modes and the vibration modes are the high frequency modes. The dynamics of the system can then be divided into two

sub-systems. The low frequency sub-system has the same order as that of the rigid body sub-system. The low frequency variables are considered as constant parameters for the high frequency sub-system.

An alternative method for modeling the arm system is the frequency domain approach. This method can be used to develop a transfer matrix model using the Euler-Bernoulli's beam equation for a uniform beam. The disadvantage of this method is that it is not possible to include the interaction between the gross motion and vibration of the arm in the model. Hence, the model can only be considered as an approximate method (Azad 1994; Tokhi and Azad 1996a).

An analytical model based on the Lagrange's equation and modal expansion method has previously been proposed (Tokhi and Azad 1996a). This model contains an infinite number of natural modes. It is used to develop a state space and equivalent frequency domain model of the system. These models are used as background knowledge for the identification and modeling process in this study.

The finite difference (FD) method has been used to obtain an efficient numerical method of solving the governing dynamic equation, partial differential equation (PDE), of the flexible arm system through discretisation, both, in time and space (distance) coordinates of the system. The algorithm proposed in this study allows the inclusion of distributed actuator and sensor terms in the PDE and modification of boundary conditions. The development of such an algorithm for a system without the inclusion of structural damping has previously been reported (Tokhi and Azad 1995). However, to provide a more realistic characterization of a flexible arm, the development of a simulation environment incorporating a mode frequency dependent structural damping can be pursued.

Both open-loop and closed-loop control strategies have been considered for control of flexible arms (Tokhi and Azad 1996b). Open-loop control methods have included bang-bang torque input, low-pass filtered and *Gaussian* shaped torque inputs. Closed-loop control, on the other hand, has included joint based collocated control and end point feedback (non-collocated control).

An important aspect of the flexible arm control that has received little attention is the interaction between the rigid and flexible dynamics of the links. As the arm configuration changes, the spatial boundary conditions of the links change, thereby modifying their characteristic frequencies and modes. Carrying a load leads to a change in the natural modes. This has important implications for control design, where the performance of a controller designed on the basis of a fixed linear model of the dynamics may be seriously degraded. There are several possible options to solve this problem: a controller based on a more general model of the system, perhaps even a non-linear model, a *robust control scheme* which can maintain satisfactory level of performance despite changes in the arm dynamics, an *adaptive control scheme* which modifies the controller in line with changes in the system. Model based control can work best for a particular model of the system. The robust fixed-parameter control scheme is limited to a very narrow range of system changes. There is always a trade-off between the range of system changes and the quality of the final control. Adaptive control schemes, combining plant model and

controller adaptation, require necessary computing capability at the speed necessitated by the dynamics of the flexible arm.

It is still not clear which of the various control schemes available represents the best all-round solution for flexible arm control or even whether there is a single best solution. Unfortunately, trends towards intelligent control of flexible arm to date are not satisfactory and researches reported are very few. This area of research demands further attention from the research community.

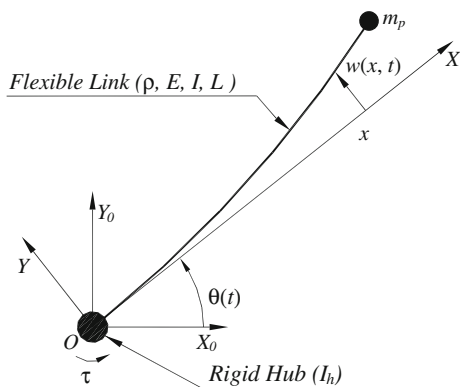
2.5 Dynamic Equations of Flexible Robotic Arm

A schematic representation of the flexible arm system considered in this work is shown in Fig. 2.6, where X_0OY_0 and XOY represent the stationary and moving coordinates respectively, $\tau(t)$ represents the applied torque at the hub. E , I , ρ , V , I_h and m_p represent the Young modulus, area moment of inertia, mass density per unit volume, cross sectional area, hub inertia and payload of the arm respectively. In this work, the motion of the arm is confined to the X_0OY_0 plane.

The flexible arm system can be modelled as a pinned-free flexible beam, incorporating an inertia at the hub and payload mass at the end-point. The model is developed through the utilisation of Lagrange equation and modal expansion method (Hasting and Book 1987). For an angular displacement θ and an elastic deflection u , the total displacement $y(x, t)$ of a point along the arm at a distance x from the hub can be described as a function of both the rigid body motion $\theta(t)$ and elastic deflection $u(x, t)$ measured from the line OX . The dynamic equations of motion of the arm can be obtained using the Hamilton's extended principle (Meirovitch 1967) with the associated kinetic, potential and dissipated energies of the system. Ignoring the effects of the rotary inertia and shear deformation, a fourth order PDE representing the arm motion can be obtained as (Azad 1994)

$$EI \frac{\partial^4 u(x, t)}{\partial x^4} + \rho \frac{\partial^2 u(x, t)}{\partial t^2} = -\rho x \ddot{\theta} \quad (2.11)$$

Fig. 2.6 Schematic representation of the single-link flexible arm



where $u(x, t)$ is the deflection of the link, ρ is density of the material, EI is the flexural stiffness. This equation is very difficult to solve because of the third term on the left-hand side.

To obtain the corresponding boundary conditions, the following must hold

- The displacement at the hub $\{u(0, t)\}$ must be zero,
- The total forces at the hub must be the same with the applied torque,
- The shear force at the end-point must be equal to $M_p \frac{\partial^2 u(x, t)}{\partial t^2}$ (Tse et al. 1980).
- The stress at the end-point must be zero, that is, no force should be present at the free end;

$$\begin{aligned}
 u(0, t) &= 0 \\
 I_h \frac{\partial^3 u(0, t)}{\partial t^2 \partial x} - EI \frac{\partial^2 u(0, t)}{\partial x^2} &= \tau(t) \\
 M_p \frac{\partial^2 u(l, t)}{\partial t^2} - EI \frac{\partial^3 u(l, t)}{\partial x^3} &= 0 \\
 EI \frac{\partial^2 u(l, t)}{\partial x^2} &= 0
 \end{aligned} \tag{2.12}$$

where l is the length of the arm.

Equation (2.11) with the corresponding boundary conditions in Eq. (2.12) represents the dynamic equation of motion of the flexible arm system assuming no damping in the system. In practice, however, such an effect is always present in the system. There are several possible forms of damping within the system. To incorporate damping into the governing dynamic equation of the system, a mode frequency dependent damping term proportional to $\frac{\partial^3 u(x, t)}{\partial x^2 \partial t}$ can be introduced (Davis and Hirschorn 1988). Equation (2.11) can thus be modified to yield

$$EI \frac{\partial^4 u(x, t)}{\partial x^4} + \rho \frac{\partial^2 u(x, t)}{\partial t^2} - D_S \frac{\partial^3 u(x, t)}{\partial x^2 \partial t} = -\rho x \ddot{\theta} \tag{2.13}$$

where D_S is the resistance to strain velocity, that is, rate of change of strain and $D_S \frac{\partial^3 u(x, t)}{\partial x^2 \partial t}$ represents the resulting damping moment dissipated in the arm structure during its dynamic operation. The corresponding boundary conditions are:

$$\begin{aligned}
 u(0, t) &= 0 \\
 I_h \frac{\partial^3 u(0, t)}{\partial t^2 \partial x} - EI \frac{\partial^2 u(0, t)}{\partial x^2} &= \tau(t) \\
 M_p \frac{\partial^2 u(l, t)}{\partial t^2} - EI \frac{\partial^3 u(l, t)}{\partial x^3} &= 0 \\
 EI \frac{\partial^2 u(l, t)}{\partial x^2} &= 0
 \end{aligned} \tag{2.14}$$

Substituting for $u(x, t)$ using total displacement $y(x, t) = x\theta(t) + u(x, t)$, Eq. (2.13), the boundary conditions, manipulating and simplifying yields the governing equation of motion of the arm in terms of $y(x, t)$ as

$$EI \frac{\partial^4 y(x, t)}{\partial x^4} + \rho \frac{\partial^2 y(x, t)}{\partial t^2} - D_s \frac{\partial^3 y(x, t)}{\partial x^2 \partial t} = 0 \quad (2.15)$$

Equation (2.15) gives the fourth-order PDE which represents the dynamic equation describing the motion of the flexible arm. To solve this equation and develop a suitable simulation environment characterising the behaviour of the system, the Finite difference (FD) method can be used. Thus, a set of equivalent difference equations defined by the central finite difference quotients of the FD method are obtained by discretising the PDE in Eq. (2.15) with its associated boundary and initial conditions. The process involves dividing the arm into N sections each of length Δx and considering the deflection of each section at sample times Δt . In this manner, a solution of the PDE is obtained by generating the central difference formulae for the partial derivative terms of the response $y(x, t)$ of the arm at points $x = i.\Delta x$, $t = j.\Delta t$ (Azad 1994; Burden and Faires 1989; Lapidus 1982):

$$\begin{aligned} \frac{\partial^2 y(x, t)}{\partial t^2} &= \frac{y_{i,j+1} - 2y_{i,j} + y_{i,j-1}}{\Delta t^2} \\ \frac{\partial^2 y(x, t)}{\partial x^2} &= \frac{y_{i+1,j} - 2y_{i,j} + y_{i-1,j}}{\Delta x^2} \\ \frac{\partial^3 y(x, t)}{\partial x^3} &= \frac{y_{i+2,j} - 2y_{i+1,j} + 2y_{i-1,j} - y_{i-2,j}}{2\Delta x^3} \\ \frac{\partial^4 y(x, t)}{\partial x^4} &= \frac{y_{i+2,j} - 4y_{i+1,j} + 6y_{i,j} - 4y_{i-1,j} + y_{i-2,j}}{\Delta x^4} \\ \frac{\partial^3 y(x, t)}{\partial t^2 \partial x} &= \frac{y_{i,j+1} - 2y_{i,j} + y_{i,j-1} - y_{i-1,j+1} + 2y_{i-1,j} - y_{i-1,j-1}}{\Delta x \Delta t^2} \\ \frac{\partial^3 y(x, t)}{\partial x^2 \partial t} &= \frac{y_{i+1,j} - 2y_{i,j} + y_{i-1,j} - y_{i+1,j-1} + 2y_{i,j-1} - y_{i-1,j-1}}{\Delta t \Delta x^2} \end{aligned} \quad (2.16)$$

where, $y_{i,j}$ represents the response $y(x, t)$ at $x = i\Delta x$ and $t = j\Delta t$ or $y(x_i, t_j)$. A time-space discretisation is adopted in the evaluation of the response of the arm.

2.5.1 Development of the Simulation Algorithm

A solution of the PDE in Eq. (2.15) can be obtained by substituting for $\frac{\partial^2 y}{\partial t^2}$, $\frac{\partial^4 y}{\partial x^4}$ and $\frac{\partial^3 y}{\partial x^2 \partial t}$ from Eq. (2.16) and simplifying to yield

$$\begin{aligned} \frac{EI}{\Delta x^4} [y_{i+2,j} - 4y_{i+1,j} + 6y_{i,j} - 4y_{i-1,j} + y_{i-2,j}] + \frac{\rho}{\Delta t^2} [y_{i,j+1} - 2y_{i,j} + y_{i,j-1}] \\ - \frac{D_s}{\Delta x^2 \Delta t} [y_{i+1,j} - 2y_{i,j} + y_{i-1,j} - y_{i+1,j-1} + 2y_{i,j-1} - y_{i-1,j-1}] = 0 \end{aligned}$$

or

$$y_{i,j+1} = -c[y_{i+2,j} + y_{i-2,j}] + b[y_{i+1,j} + y_{i-1,j}] + a y_{i,j} - y_{i,j-1} + d[y_{i+1,j} - 2y_{i,j} + y_{i-1,j} - y_{i+1,j-1} + 2y_{i,j-1} - y_{i-1,j-1}] \quad (2.17)$$

where $a = 2 - \frac{6EI\Delta t^2}{\rho\Delta x^4}$; $b = \frac{4EI\Delta t^2}{\rho\Delta x^4}$; $c = \frac{EI\Delta t^2}{\rho\Delta x^4}$; $d = \frac{Ds\Delta t}{\rho\Delta x^2}$.

Equation (2.17) gives the displacement of section i of the arm at time step $j + 1$. It follows from this equation that, to obtain the displacements $y_{n-1,j+1}$ and $y_{n,j+1}$, the displacements of the fictitious points $y_{n+2,j}$, $y_{n+1,j}$ and $y_{n+1,j-1}$ are required. These can be obtained using the boundary conditions related to the dynamic equation of the flexible arm. The discrete form of the corresponding boundary conditions are:

$$y_{0,j} = 0 \quad (2.18)$$

$$y_{-1,j} = y_{1,j} + \frac{\Delta x I_h}{EI\Delta t^2} [y_{1,j+1} - 2y_{1,j} + y_{1,j-1}] + \frac{\Delta x^2}{EI} \tau(j) \quad (2.19)$$

$$y_{n+2,j} = 2y_{n+1,j} - 2y_{n-1,j} + y_{n-2,j} + \frac{2\Delta x^3 M_p}{\Delta t^2 EI} [y_{n,j+1} - 2y_{n,j} + y_{n,j-1}] \quad (2.20)$$

$$y_{n+1,j} = 2y_{n,j} - y_{n-1,j} \quad (2.21)$$

2.5.2 Hub Displacement

Note that the torque is applied at the hub of the flexible arm. Thus, $\tau(i,j) = 0$ for $i \geq 1$. Using Eqs. (2.17) and (2.18), the displacement $y_{1,j+1}$ can be obtained as

$$y_{1,j+1} = -c[y_{3,j} + y_{-1,j}] + b y_{2,j} + a y_{1,j} - y_{1,j-1} + d[y_{2,j} - 2y_{1,j} - y_{2,j-1} + 2y_{1,j-1}] \quad (2.22)$$

Substituting for $y_{-1,j}$ from Eq. (2.19) into Eq. (2.22) and simplifying yields

$$y_{1,j+1} = K_1 y_{1,j} + K_2 y_{2,j} + K_3 y_{3,j} + K_4 y_{1,j-1} + K_5 y_{2,j-1} + K_6 \tau(j) \quad (2.23)$$

where

$$\begin{aligned} K_1 &= \frac{c\Delta t^2 EI + 2c\Delta x I_h + (a-2d)\Delta t^2 EI}{\Delta t^2 EI + c\Delta x I_h} & K_4 &= -\frac{c\Delta x I_h + (1-2d)\Delta t^2 EI}{\Delta t^2 EI + c\Delta x I_h} \\ K_2 &= \frac{(b+d)\Delta t^2 EI}{\Delta t^2 EI + c\Delta x I_h} & K_5 &= -\frac{d\Delta t^2 EI}{\Delta t^2 EI + c\Delta x I_h} \\ K_3 &= -\frac{c\Delta t^2 EI}{\Delta t^2 EI + c\Delta x I_h} & K_6 &= \frac{c\Delta x^2 \Delta t^2}{\Delta t^2 EI + c\Delta x I_h} \end{aligned}$$

2.5.3 End-Point Displacement

Using Eq. (2.17) for $i = n - 1$, yields the displacement $y_{n-1,j-1}$ as

$$y_{n-1,j+1} = -c[y_{n-3,j} + y_{n+1,j}] + b[y_{n,j} + y_{n-2,j}] + a y_{n-1,j} - y_{n-1,j-1} + d[y_{n,j} - 2y_{n-1,j} + y_{n-2,j} - y_{n,j-1} + 2y_{n-1,j-1} - y_{n-2,j-1}] \quad (2.24)$$

Similarly, using Eq. (2.17) for $i = n$, yields the displacement $y_{n,j+1}$ as

$$y_{n,j+1} = -c[y_{n-2,j} + y_{n+2,j}] + b[y_{n+1,j} + y_{n-1,j}] + a y_{n,j} - y_{n,j-1} + d[y_{n+1,j} - 2y_{n,j} + y_{n-1,j} - y_{n+1,j-1} + 2y_{n,j-1} - y_{n-1,j-1}] \quad (2.25)$$

The fictitious displacements $y_{n+1,j}$ and $y_{n+2,j}$, appearing in Eqs. (2.24) and (2.25), can be obtained using the boundary conditions in Eqs. (2.20) and (2.21). $y_{n+1,j-1}$ can easily be obtained by shifting $y_{n+1,j}$ from time step j to time step $j - 1$. Substituting for $y_{n+1,j}$ from Eq. (2.21) into Eq. (2.24) yields the displacement $y_{n-1,j+1}$ as

$$y_{n-1,j+1} = K_7 y_{n-3,j} + K_8 y_{n-2,j} + K_9 y_{n-1,j} + K_{10} y_{n,j} + K_{11} y_{n-2,j-1} + K_{12} y_{n-1,j-1} + K_{13} y_{n,j-1} \quad (2.26)$$

where

$$\begin{aligned} K_7 &= -c & K_{11} &= -d \\ K_8 &= (b + d) & K_{12} &= -(1 - 2d) \\ K_9 &= (a + c - 2d) & K_{13} &= -d \\ K_{10} &= -(2c - b - d) \end{aligned}$$

Similarly, substituting for $y_{n+2,j}$ and $y_{n+1,j}$ from Eqs. (2.20) and (2.21) into Eq. (2.25), and simplifying yields the displacement $y_{n,j+1}$ as

$$y_{n,j+1} = K_{14} y_{n-2,j} + K_{15} y_{n-1,j} + K_{16} y_{n,j} + K_{17} y_{n,j-1} \quad (2.27)$$

where

$$\begin{aligned} K_{14} &= \frac{-2c\Delta t^2 EI}{\Delta t^2 EI + 2c\Delta x^3 M_P} \\ K_{15} &= \frac{4c\Delta t^2 EI}{\Delta t^2 EI + 2c\Delta x^3 M_P} \\ K_{16} &= \frac{\Delta t^2 EI}{\Delta t^2 EI + 2c\Delta x^3 M_P} \left\{ a + 2b - 4c + \frac{4c\Delta x^3 M_P}{\Delta t^2 EI} \right\} \\ K_{17} &= \frac{-\Delta t^2 EI}{\Delta t^2 EI + 2c\Delta x^3 M_P} \left\{ \frac{2c\Delta x^3 M_P}{\Delta t^2 EI} + 1 \right\} \end{aligned}$$

Equations (2.17), (2.23), (2.26) and (2.27) represent the dynamic equation of the arm for all the grid points (stations) at specified instants of time t in the presence of hub inertia and payload.

$$y_{i,j+1} = -c[y_{i+2,j} + y_{i-2,j}] + b[y_{i+1,j} + y_{i-1,j}] + ay_{i,j} - y_{i,j-1} + d[y_{i+1,j} - 2y_{i,j} + y_{i-1,j} - y_{i+1,j-1} + 2y_{i,j-1} - y_{i-1,j-1}] \quad (2.28)$$

$$y_{1,j+1} = K_1y_{1,j} + K_2y_{2,j} + K_3y_{3,j} + K_4y_{1,j-1} + K_5y_{2,j-1} + K_6\tau(j) \quad (2.29)$$

$$y_{n-1,j+1} = K_7y_{n-3,j} + K_8y_{n-2,j} + K_9y_{n-1,j} + K_{10}y_{n,j} + K_{11}y_{n-2,j-1} + K_{12}y_{n-1,j-1} + K_{13}y_{n,j-1} \quad (2.30)$$

$$y_{n,j+1} = K_{14}y_{n-2,j} + K_{15}y_{n-1,j} + K_{16}y_{n,j} + K_{17}y_{n,j-1} \quad (2.31)$$

2.5.4 Matrix Formulation

Using matrix notation, Eqs. (2.28)–(2.31) can be written in a compact form as

$$\mathbf{Y}_{i,j+1} = \mathbf{A}\mathbf{Y}_{i,j} + \mathbf{B}\mathbf{Y}_{i,j-1} + \mathbf{C}\mathbf{F} \quad (2.32)$$

where $\mathbf{Y}_{i,j+1}$ is the displacement of grid points $i = 1, 2, \dots, n$ of the arm at time step $j + 1$, $\mathbf{Y}_{i,j}$ and $\mathbf{Y}_{i,j-1}$ are the corresponding displacements at time steps j and $j - 1$ respectively. \mathbf{A} and \mathbf{B} are constant $n \times n$ matrices whose entries depend on the flexible arm specification and the number of sections the arm is divided into, \mathbf{C} is a constant matrix related to the given input torque and \mathbf{F} is an $n \times 1$ matrix related to the time step Δt and mass per unit length of the flexible arm;

$$\mathbf{Y}_{i,j+1} = \begin{bmatrix} y_{1,j+1} \\ y_{2,j+1} \\ \vdots \\ y_{n,j+1} \end{bmatrix}, \mathbf{Y}_{i,j} = \begin{bmatrix} y_{1,j} \\ y_{2,j} \\ \vdots \\ y_{n,j} \end{bmatrix}, \mathbf{Y}_{i,j-1} = \begin{bmatrix} y_{1,j-1} \\ y_{2,j-1} \\ \vdots \\ y_{n,j-1} \end{bmatrix} \quad (2.33)$$

$$\mathbf{A} = \begin{bmatrix} K_1 & K_2 & K_3 & 0 & 0 & \dots & 0 & 0 \\ (b+d) & (a-2d) & (b+d) & -c & 0 & \dots & 0 & 0 \\ -c & (b+d) & (a-2d) & (b+d) & -c & \dots & 0 & 0 \\ \vdots & \ddots & \ddots & \ddots & \ddots & \ddots & \ddots & \vdots \\ 0 & 0 & \dots & -c & b+d & a-2d & b+d & -c \\ 0 & 0 & \dots & 0 & K_7 & K_8 & K_9 & K_{10} \\ 0 & 0 & \dots & 0 & 0 & K_{14} & K_{15} & K_{16} \end{bmatrix} \quad (2.34)$$

$$\mathbf{B} = \begin{bmatrix} K_4 & K_5 & 0 & 0 & 0 & \cdots & 0 & 0 \\ -d & 2d-1 & -d & 0 & 0 & \cdots & 0 & 0 \\ 0 & -d & 2d-1 & -d & 0 & \cdots & 0 & 0 \\ \vdots & \ddots & \ddots & \ddots & \ddots & \ddots & \ddots & \vdots \\ 0 & 0 & \cdots & 0 & -d & 2d-1 & -d & 0 \\ 0 & 0 & \cdots & 0 & 0 & K_{11} & K_{12} & K_{13} \\ 0 & 0 & \cdots & 0 & 0 & 0 & 0 & K_{17} \end{bmatrix} \quad (2.35)$$

$$\mathbf{C} = \tau(j), \mathbf{F} = [K_6 \quad 0 \quad \cdots \quad 0]^T \quad (2.36)$$

2.5.5 State-Space Formulation

A state-space formulation of the dynamic equation of the arm can be constructed by referring to the matrix formulation. Using the notation for simulation of discrete-time linear systems, the dynamic equations of the flexible arm can be written as

$$\begin{aligned} x(n+1) &= \mathbf{P}x(n) + \mathbf{Q}u \\ y(n) &= \mathbf{R}x(n) + \mathbf{S}u \end{aligned} \quad (2.37)$$

where $\mathbf{P} = \begin{bmatrix} A & \text{vline} & B \\ I_{N \times N} & & 0_{N \times N} \end{bmatrix}$, $\mathbf{Q} = \begin{bmatrix} C \\ 0_{N \times 1} \end{bmatrix}$, $\mathbf{R} = [I_N \quad 0_N]$, $\mathbf{S} = [0_{2N}]$

$$u = [\tau \quad 0 \quad \cdots \quad 0]^T, y(n) = [x(1, n) \cdots x(N, n), x(1, n-1) \cdots x(N, n-1)]$$

N represents the number of sections.

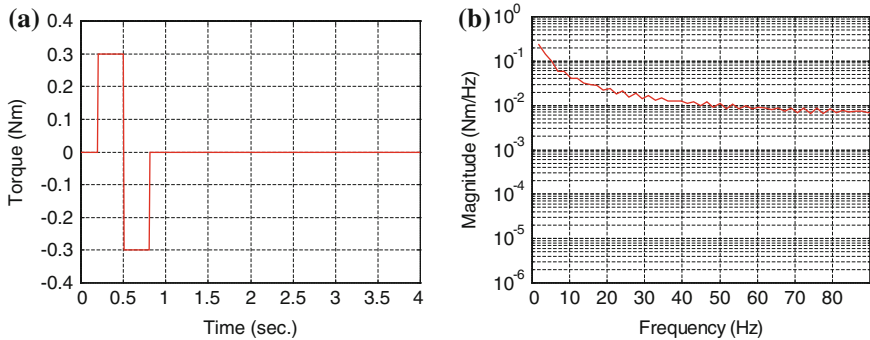


Fig. 2.7 The bang-bang torque input. Time-domain (a); Spectral-density (b)

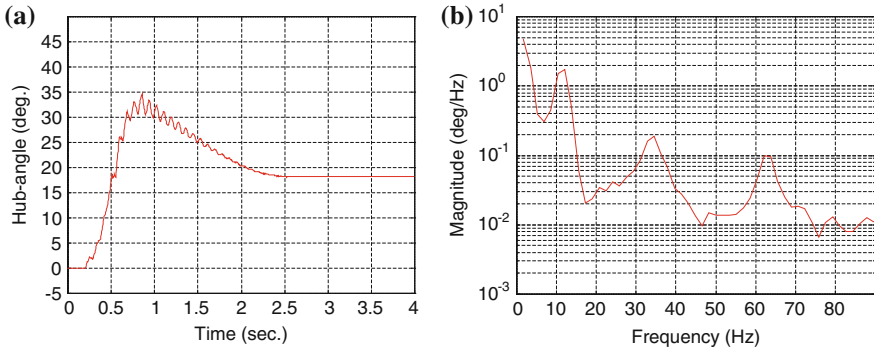


Fig. 2.8 The hub-angle. Time-domain (a); Spectral-density (b)

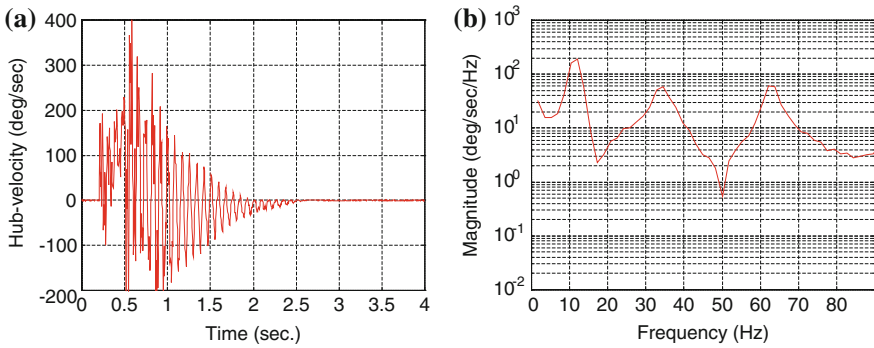
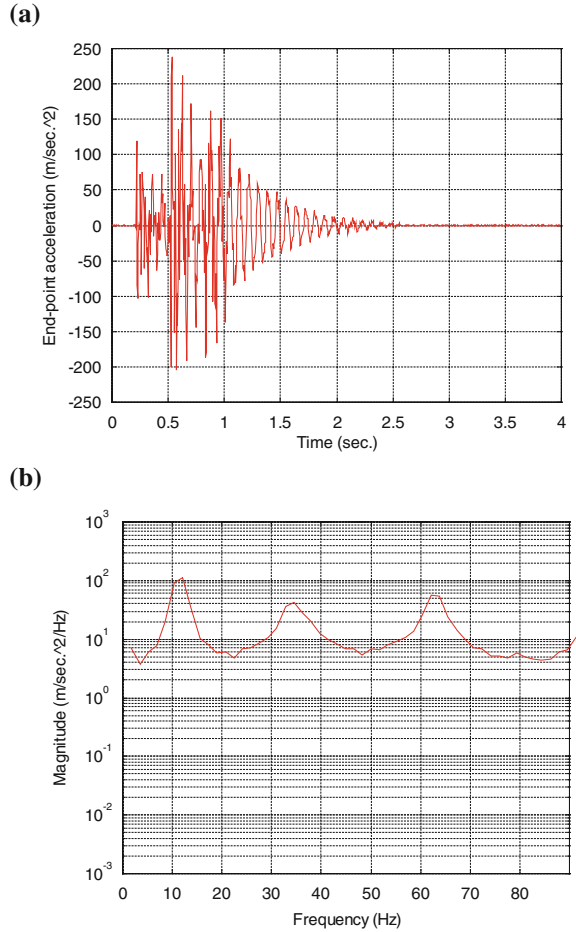


Fig. 2.9 The hub-velocity. Time-domain (a); Spectral-density (b)

2.6 Some Simulation Results

To identify an unknown process some knowledge of the process and signals is required. The simplest way is to apply a signal and record the system's response. This data set can best describe the characteristic behaviour of the flexible arm. There are various types of signals, which can be used as inputs to the system. Two types of signals, namely a bang-bang and composite PRBS are widely used for this purpose. In this experiment a bang-bang signal is used. It has been reported that the vibration of the flexible arm is dominated by the first few (commonly two) resonance modes. Anti-aliasing filters with cut-off frequency of 100 Hz are used for the four outputs namely, the hub-angle output, the hub-velocity output, the end-point acceleration output and the motor-current output.

Fig. 2.10 The end-point acceleration. Time-domain (a); Spectral-density (b)

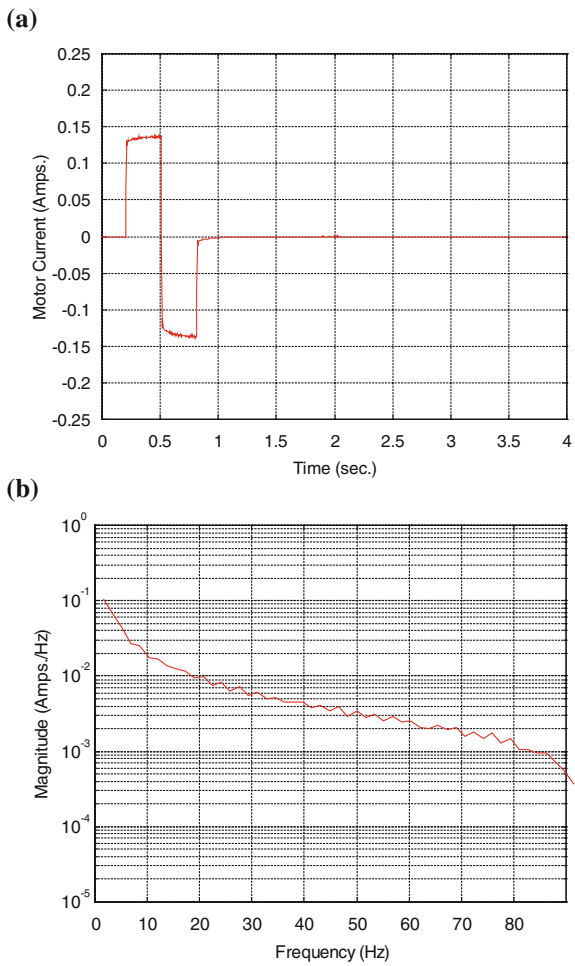


2.6.1 Bang-Bang Signal

The first attempt is to excite the flexible arm using a bang-bang torque input signal. This is shown in Fig. 2.7. This has a positive (acceleration) and negative (deceleration) period allowing the arm to, initially, accelerate and then decelerate and eventually stop at a target location. An amplitude of ± 0.3 Nm and duration of 0.6 s is chosen for the bang-bang signal in this experiment. The system response as hub angle, hub velocity, end-point acceleration and motor current with the corresponding spectral densities, are observed for 4 s.

Figure 2.8 shows the trajectory of the hub displacement due to the bang-bang torque input. Theoretically, the energy of the corresponding bang-bang torque would equally distribute for acceleration and deceleration phases of the system.

Fig. 2.11 The motor current. Time-domain (a); Spectral-density (b)



This means that there would be no further rigid body movement after the braking phase of the bang-bang torque has ended, although vibrations or oscillations might take place during this period. Due to problems, which commonly occur under real conditions, for example, due to shaft motor frictions, which lead to the dead zone problem, the response of the hub to the bang-bang torque gives a different behaviour. The displacement has reached 30–35° but then moved back to 18°.

Figures 2.9, 2.10 and 2.11 show the hub velocity, the end-point acceleration and the motor current output with corresponding spectral densities.

2.7 Summary

A general description and characterization of the flexible arm system have been presented. The system consists of two main parts: a flexible arm and measuring devices. The flexible arm is clamped at the hub to a drive motor. The end-point is assumed to carry a payload, and the vibrations in this position, are measured using an accelerometer. A printed armature motor has been carefully chosen as the drive motor since this type of motor has significant advantages compared to other types of motor. It delivers high torque instantly, is capable of producing rapid acceleration and deceleration, and provides extremely smooth torque with no 'cogging'. The motor drive amplifier has cautiously been selected to deliver a current proportional to the input voltage: that is, for a given amount of input voltage it can produce a proportional current output to the motor. The hub position and velocity are measured using a shaft encoder and a tachometer respectively. A numerical method of solution of the governing PDE describing the characteristic behaviour of a flexible arm system incorporating the hub inertia, payload and damping has been presented. Finally a state space model has been presented.

References

- Asada H, Stoline JE (1986) Robot analysis and control. John Wiley, New York
- Azad AKM (1994) Analysis and design of control mechanisms for flexible arm systems, Ph.D. thesis, Department of Automatic Control and Systems Engineering, The University of Sheffield, UK
- Book WJ (1984) Recursive lagrangian dynamics of flexible arm arms. *Int J Robot Res* 3(3):87–101
- Burden RL, Faires JD (1989) Numerical analysis. PWS-KENT Publishing Company, Boston
- Cannon RH, Schmitz E (1984) Initial experiments on the end-point control of a flexible one-link robot. *Int J Robot Res* 3:62–75
- Davis JH, Hirschorn RM (1988) Tracking control of flexible robot link. *IEEE Trans Autom Control* 33:238–248
- Fu KS, Gonzalez RC, Lee CSG (1987) Robotics: control, sensing, vision and intelligence. McGraw-Hill, New York
- Hastings GG, Book WJ (1987) A linear dynamic model for flexible robotics arm. *IEEE Control Syst Mag* 7:61–64
- Hastings GG, Ravishankar BN (1988) An experimental system for investigation of flexible link experiencing general motion. In: *Proceedings of the conference on decision and control*, pp 1003–1008
- Khosla PK, Kanade T (1988) Experimental evaluation of non-linear feedback and feed forward control schemes for arms. *Int J Robot Res* 7(1):790–798
- Kuo BC, Tal J (ed) (1978) DC motors and control systems. SRL Publishing Company, Champaign, Illinois
- Lapidus L (1982) Numerical solution of partial differential equations in science and engineering. John Wiley, New York
- Meirovitch L (1967) Analytical methods in vibrations. Macmillan, New York
- Schilling RJ (1990) Fundamentals of robotics analysis and control. Prentice Hall, Englewood Cliffs

- Seraji H, Moya MM (1987) Position control for non-linear multiple link robots, NASA technical brief 11(3):119
- Tokhi MO, Azad AKM (1995) Real-time finite difference simulation of a single-link flexible arm system incorporating hub inertia and payload. *Proc IMechE-I J Syst Control Eng* 209(11):21–33
- Tokhi MO, Azad AKM (1996a) Modeling of a single-link flexible arm system: theoretical and practical investigations. *Robotica* 14:91–102
- Tokhi MO, Azad AKM (1996b) Control of flexible arm systems. *Proc Inst Mech Eng* 210:113–130
- Tokhi MO, Azad AKM (1997) Design and development of an experimental flexible arm system. *Robotica* 15(3):283–292
- Tse FS, Morse IE, Hinkle TR (1980) *Mechanical vibrations theory and applications*. Allyn and Bacon Inc., Boston

<http://www.springer.com/978-3-319-02134-8>

Intelligent Control

A Hybrid Approach Based on Fuzzy Logic, Neural
Networks and Genetic Algorithms

Siddique, N.

2014, XVII, 282 p. 158 illus., 55 illus. in color.,

Hardcover

ISBN: 978-3-319-02134-8